Earth and Planetary Science Letters 295 (2010) 91–103

Contents lists available at ScienceDirect

Earth and Planetary Science Letters

journal homepage: www.elsevier.com/locate/epsl

Episodic growth and homogenization of plutonic roots in arc volcanoes from combined U–Th and (U–Th)/He zircon dating

Axel K. Schmitt [a,*], Daniel F. Stockli [b], Jan M. Lindsay [c], Richard Robertson [d], Oscar M. Lovera [a], Roman Kislitsyn [b]

[a] Department of Earth and Space Sciences, University of California Los Angeles, 595 Charles Young Drive E, Los Angeles CA 90095, USA
[b] Department of Geology, University of Kansas, 120 Lindley Hall, 1475 Jayhawk Boulevard, Lawrence, KS 66045-7613, USA
[c] School of Environment, The University of Auckland, Private Bag 92019, Auckland 1142, New Zealand
[d] The Seismic Research Centre, The University of the West Indies, St. Augustine, Trinidad and Tobago

ARTICLE INFO

Article history:
Received 15 January 2010
Received in revised form 15 March 2010
Accepted 18 March 2010
Available online 5 May 2010

Editor: R.W. Carlson

Keywords:
zircon residence time
Quaternary geochronology
arc volcanism
magma chambers
plutons

ABSTRACT

Tracing the fate of unerupted magma is challenging because plutonic roots of young volcanoes are largely inaccessible. Here we develop the use of zircon age spectra to determine crystal provenance and source rocks for volcanic products, in analogy to detrital crystals in sediments. U–Th zircon crystallization ages for the Soufrière Volcanic Complex, Saint Lucia (Lesser Antilles) frequently predate their eruption as determined from combined U–Th and (U–Th)/He zircon dating. The oldest dated eruptions are 273 ± 15 ka and 264 ± 8 ka (1σ uncertainty) for Morne Bonin dacite and Bellevue pumice deposit, respectively. The most recent eruptions formed morphologically pristine domes in the center of the Qualibou depression (Belfond: 13.6 ± 0.4 ka; Terre Blanche: 15.3 ± 0.4 ka). U–Th (U–Pb) zircon crystallization ages determined for crystal rims and interiors range between near-eruption ages to ~600 ka. Older xenocrysts are absent. Zircon crystallization age distributions are complex, yet systematic: crystal rim ages in the most recently erupted volcanic rocks match those of co-erupted plutonic inclusions, whereas crystal interiors are equivalent to the cumulative distribution of zircon ages from older eruptions. This is evidence that silicic lava domes and pyroclastic flows share a common source that is located underneath the Qualibou depression, where the intrusive roots of this long-lived arc volcanic system became homogenized through thermal and mechanical reprocessing of individual batches of unerupted magma from earlier volcanic episodes within timescales of <100 ka.

1. Introduction

Differentiated plutons are a volumetrically important component of the upper crust in oceanic and continental arcs (e.g., Kay and Kay, 1985). They represent the intrusive equivalents of magmas that feed explosive silicic volcanism (e.g., Bachmann et al., 2007). Crustal growth underneath arc volcanoes is implicit in estimates of intrusive to extrusive ratios in volcanic systems that exceed unity (e.g., 5:1; White et al., 2006), but quantification is frustrated by large uncertainties in these ratios. The generation of arc plutons by fractional crystallization, for example, requires a ratio of ~10:1 of intrusive cumulates over differentiated magma (Perfit et al., 1980), whereas thermal models predict ratios for immobile intrusions over eruptible magma approaching ~2:1 for aggregated sill complexes at steady state and high magma input rates (Annen, 2009).

In order to more precisely constrain crustal growth rates in arcs, it is important to trace the fate of unerupted magma. This is challenging because the components of volcanic–plutonic systems are typically inaccessible (in recent arcs) or incompletely preserved (in ancient arcs). Previous workers (Coleman et al., 2004; Matzel et al., 2006; Miller et al., 2007; Michel et al., 2008; Schaltegger et al., 2009) have interpreted inter-crystal variability of thermal ionization mass spectrometry (TIMS) U–Pb zircon ages from plutonic rocks exposed in old magmatic arcs as evidence for protracted magma presence and incremental pluton growth over Ma timescales that are equivalent to those of volcanic activity of composite arc volcanoes (e.g., Grunder et al., 2006). Many modern volcanic systems, however, show eruptive cycles on much shorter timescales than are resolvable by U–Pb zircon geochronology. TIMS zircon ages are also inevitably biased because the technique averages age domains within individual crystals or fragments, or obliterates them through mechanical or chemical abrasion pre-treatment. Moreover, the number of grains that are typically analyzed in these studies is small (e.g., five crystals per sample in Michel et al. (2008)), leaving uncertainties about whether such sampling is representative.

* Corresponding author.
E-mail address: axel@oro.ess.ucla.edu (A.K. Schmitt).

0012-821X/$ – see front matter © 2010 Elsevier B.V. All rights reserved.
doi:10.1016/j.epsl.2010.03.028

Here, we apply secondary ionization mass spectrometry (SIMS) U–Th and U–Pb zircon dating, and combine it with (U–Th)/He zircon geochronology in order to reconstruct the eruptive and intrusive history of the Soufrière Volcanic Center (SVC), Saint Lucia (Lesser Antilles arc). This is possible through $^{238}U–^{230}Th$ zircon rim analysis by depth profiling which offers optimal spatial resolution at µm scale, and preserves sufficient material for subsequent (U–Th)/He analysis. We also developed statistical modeling of large sample populations (450 ages on 385 individual crystals) that allows fingerprinting of crystal populations in individual and composite samples. This quantitative approach facilitates comparison between complex zircon crystallization age populations that are interpreted as the result of episodic assembly and recycling of a subvolcanic plexus of intermediate intrusions.

2. Geologic background

The island of Saint Lucia (620 km^2 area) is located in the southern part of the Lesser Antilles arc, which is formed by slow (~2 cm/a; DeMets et al., 2000) subduction of Atlantic oceanic crust underneath the Caribbean plate. The arc is built upon oceanic crust and possibly Early Cenozoic accretionary wedge sediments from an ancestral subduction zone (Macdonald et al., 2000). North of Martinique, the Lesser Antilles arc bifurcates into the eastern volcanically inactive Limestone Caribbees and the western Volcanic Caribbees (Macdonald et al., 2000). Volcanic activity of the older, eastern arc (forming the Limestone Caribbees) initiated in the Eocene and ceased following a change in subduction angle during the late Neogene (Burke, 1988). From the Miocene onward volcanism migrated westward, resulting in the modern volcanic arc with 33 recently active volcanic centers (Siebert and Simkin, 2002).

Lindsay (2005) categorized the volcanic rocks of Saint Lucia (Fig. 1) into three main groups (from older to younger):

1) eroded basalt and andesite centers;
2) dissected andesite centers; and
3) the Soufrière Volcanic Center.

The oldest radiometric ages obtained from basalts in group 1 are 15–18 Ma (Briden et al., 1979; De Kerneizon et al., 1983), although shallow marine volcaniclastic deposits in the northern part of Saint Lucia potentially date back to the Eocene. Group 2 rocks are mainly present in the forested and largely inaccessible central highlands of Saint Lucia. Limited dating of the dissected andesitic centers indicates eruption ages between 10.4 and 2.8 Ma (De Kerneizon et al., 1983). The most recent volcanic activity (represented by group 3 deposits) is concentrated in the SVC located within the southwestern part of the island (Tomblin, 1964; Roobol et al., 1983; Wohletz et al., 1986). Historic documents report a phreatic blast in the Sulphur Springs area at 1766 Common Era (C.E.), the only historical volcanic event in Saint Lucia (Fig. 1). Because of its geothermal activity and potential for violent explosive eruptions, the SVC has become the focus of volcanic hazard monitoring (Lindsay, 2005).

The SVC comprises a series of extensive pyroclastic flows, lava flows, domes with associated block-and-ash-flow deposits, and explosion craters that are located in and around the Qualibou depression (Fig. 1). This depression is about 5 km in diameter, with steep arcuate flanks in the east and it opens towards the Grenada basin in the west. The Qualibou structure is the source of submarine

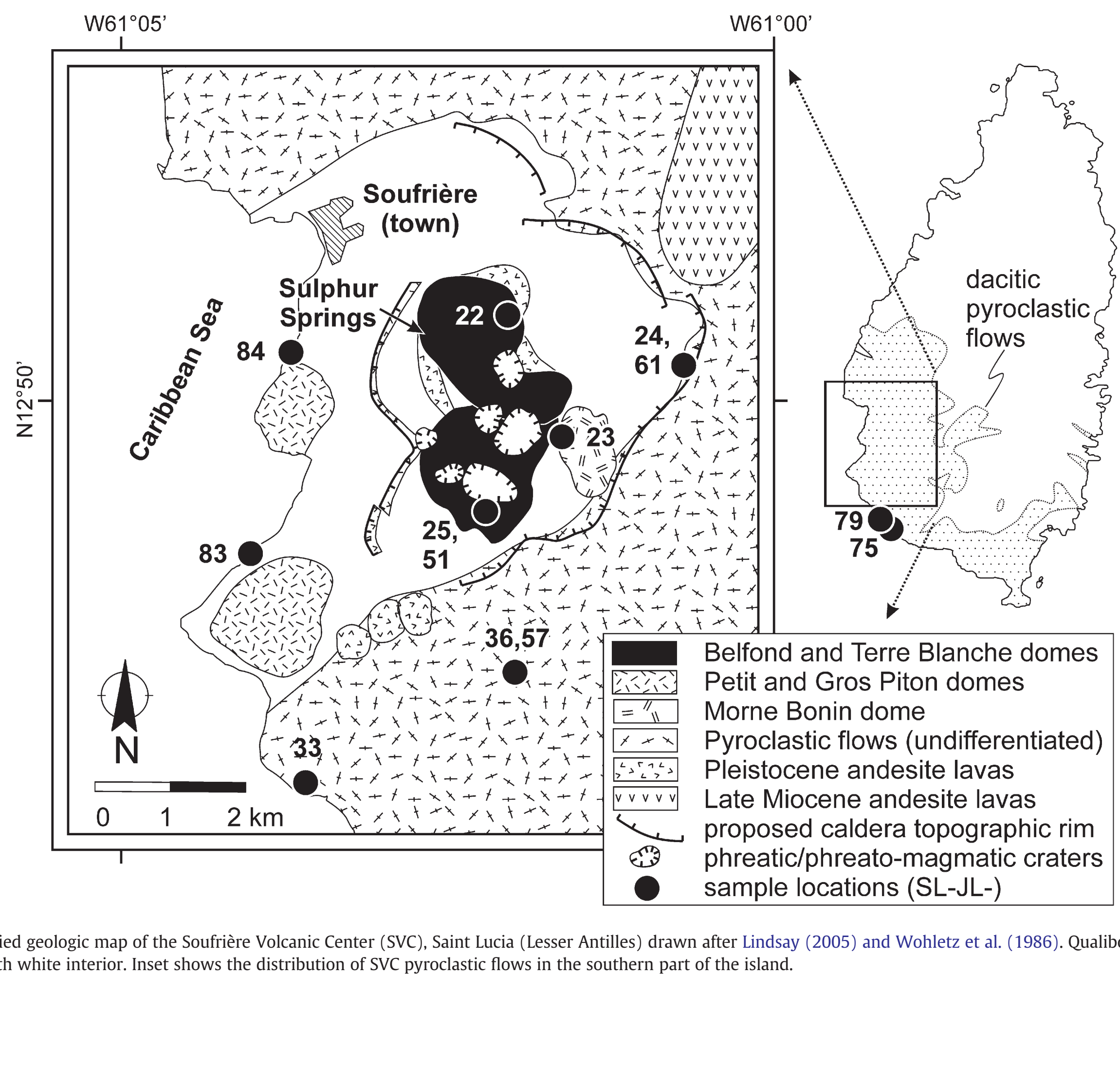

Fig. 1. Simplified geologic map of the Soufrière Volcanic Center (SVC), Saint Lucia (Lesser Antilles) drawn after Lindsay (2005) and Wohletz et al. (1986). Qualibou depression is coincident with white interior. Inset shows the distribution of SVC pyroclastic flows in the southern part of the island.

debris avalanche deposits (Deplus et al., 2001), but it is debated whether its collapse is associated with explosive volcanism (Tomblin, 1964; Wohletz et al., 1986) or gravitational flank instability (Roobol et al., 1983; Wright et al., 1984).

The oldest volcanic units within the Qualibou depression are basaltic lavas which likely correlate with group 2 lavas outside the depression. Two samples yielded K–Ar groundmass ages of 6.64 and 1.10 Ma (Samper et al., 2008). Andesitic stratovolcanoes to the N and NE of the Qualibou depression produced block-and-ash-flow deposits which are truncated at its northern margin, indicating that down-faulting postdates andesitic volcanism. Dacitic pyroclastic flow deposits form an apron around the Qualibou depression where they directly overlie paleosol and block-and-ash-flow deposits derived from older stratovolcanoes. These pyroclastic deposits have been subdivided into two map units based on the quartz content of pumice (Wright et al., 1984): the quartz-poor Choiseul tuff and quartz-rich Belfond pumice deposits. Compositionally similar dacitic lava domes comprise densely vegetated, morphologically subdued domes (e.g., Morne Bonin), and spectacularly eroded steep-flanked plugs (Gros Piton and Petit Piton; a UNESCO World Heritage Site), and a series of morphologically pristine domes (Belfond and Terre Blanche) that are also associated with active hydrothermal alteration zones and well preserved explosion craters (Fig. 1). Cognate plutonic inclusions of granodioritic composition (Arculus and Wills, 1980) are present in block-and-ash-flow deposits associated with the Belfond dome.

The relationship between domes inside the Qualibou depression and distal pyroclastic flow deposits is tenuous because of imprecise chronostratigraphic constraints. Published geochronologic data of pyroclastic deposits are mainly based on ^{14}C dating of charred tree logs (Lindsay, 2005) and range between ~20 ka (Belfond tuff) and >33 ka (Choiseul tuff). Published K–Ar dates for dacitic domes inside the Qualibou depression (Terre Blanche, Belfond, Gros Piton, Petit Piton, Morne Bonin) range between 3 ± 3 ka for Terre Blanche and 95 ± 2 ka for Gros Piton (Samper et al., 2008). A K–Ar whole-rock age of 5.3 Ma for the morphologically pristine Belfond dome is geologically unreasonable (De Kerneizon et al., 1983). Because of this wide range in ages, it remained ambiguous whether the pyroclastic flows originated from within the Qualibou depression (Wohletz et al., 1986) or from an unidentified source in the central highlands (Wright et al., 1984).

We have sampled lava and pumice from a suite of lava flows, lava domes, and pyroclastic flow deposits that include the stratigraphically oldest and youngest units of the SVC. Crystal contents of volcanic rocks range between ~20 and 40%, with phenocrysts mostly comprising plagioclase, quartz, ±hornblende, ±orthopyroxene, and ±biotite. In addition, we included two holocrystalline amphibole-bearing granodiorite inclusions. Whole-rock SiO_2 abundances fall within a limited range between 63 and 67 wt.% (anhydrous) for pumice and lava, and are 58 and 64 wt.% for two granodiorite samples, respectively. Whole-rock Zr abundances range between 94 and 135 ppm in volcanic and plutonic rocks. Because of the abundance of Zr-depleted phenocrysts and the more evolved composition of the glass, whole-rock zircon saturation temperatures of 714–772 °C (using the thermometer of Watson and Harrison (1983)) represent a minimum for the onset of zircon crystallization (Harrison et al., 2007).

3. Methods

We followed zircon separation and SIMS U–Th and U–Pb isotopic analysis protocols for the UCLA CAMECA ims 1270 described in Schmitt et al. (2003b, 2006). Zircon crystals that were extracted from pumice samples typically had adherent glass which was removed by etching in 50% HF for approximately 1 min at room temperature. Depth profiling analysis was performed on unadulterated crystal surfaces from zircon crystals pressed into indium (In) metal. Continuous depth profiling perpendicular to growth layers offers optimal spatial resolution and avoids beam overlap onto different age domains in spot analyses at 25–30 μm lateral resolution that can produce geologically irrelevant mixed ages on sectioned grain interiors. Depth resolution of U–Th ages depends on counting uncertainties of the minor isotope ^{230}Th, and typically counts from ~2 to 5 μm intervals were integrated in order to obtain model ages at 20–30% precision (1σ).

The disadvantage of depth profiling is that slow sputter rates (~0.001 μm/s) preclude representative sampling of heterogeneous zircon populations. We therefore developed a novel protocol involving briefer rim analyses of unpolished zircon crystals at ~5 μm depth resolution ("rim" analyses). Selected grains were also analyzed after sectioning through grinding and polishing as spot analyses with 25–30 μm lateral resolution ("interior" analyses). Accuracy was monitored by interspersed analysis of equilibrium zircon standard AS3 mounted next to the unknowns (1099.1 Ma; Paces and Miller, 1993) which yielded a unity secular equilibrium ratio for (^{230}Th)/(^{238}U) = 1.006 ± 0.004 (activities denoted in parentheses; MSWD = 0.78; n = 85). Uranium concentrations were estimated from $UO^+/Zr_2O_4^+$ intensity ratios relative to zircon standard 91 500 (81.2 ppm U; Wiedenbeck et al., 1995). Ages were calculated as two-point zircon — melt model isochrons using the average of two Saint Lucia dacite whole-rock analyses with (^{230}Th)/(^{232}Th) = 0.85 ± 0.07 and (^{238}U)/(^{232}Th) = 0.72 ± 0.12 (Turner et al., 1996).

For combined U–Th and (U–Th)/He analysis (Schmitt et al., 2006), grains were extracted from the In with a steel needle, photographed, and packed into platinum tubes. He degassing and isotope dilution ICP-MS analysis of U, Th, and Sm followed methods at the University of Kansas described in Biswas et al. (2007). (U–Th)/He zircon ages for Fish Canyon tuff and Durango average 27.8 ± 0.8 Ma (relative standard deviation RSD% = 7.5%, n = 285) and 30.2 ± 1.1 Ma (RSD% = 6.8; n = 76), respectively. Based on the reproducibility of standard zircon analyses, we assigned uncertainties of 8% (1σ) to the uncorrected (U–Th)/He ages. Without correction, young (U–Th)/He zircon ages often significantly underestimate the eruption age because of uranium series disequilibrium (Farley et al., 2002). Disequilibrium corrections were applied using software developed at UCLA ("MCHeCalc"; Schmitt et al., 2010). MCHeCalc applies Monte Carlo simulations that require as input parameters the uncorrected (U–Th)/He age and uncertainties, the crystallization age and uncertainties, and the D parameter (Farley et al., 2002) at the time of crystallization. We report individual disequilibrium-corrected ages, and a Gaussian fit for the average eruption age. The Q parameter (Fig. 2; Table 1) quantifies the goodness-of-fit, whereby the average age is acceptable if Q>0.001 and n>4 (Press et al., 1988). Crystallization ages are mostly based on the measured U–Th zircon rim ages. In age-zoned crystals, the rim age is a lower limit for the bulk crystallization age. If the rim age is erroneously assigned as the bulk crystallization age to an age-zoned crystal, the eruption age will be overcorrected. Indications for overcorrection are calculated eruption age that are older than the (rim) crystallization age, and low Q values. In these cases, we instead used an average age from U–Th zircon interior analyses of the same sample, or assumed secular equilibrium for the crystal interior. Improved Q values indicate that these assumptions were justified.

3.1. Eruption ages from combined U–Th and (U–Th)/He zircon dating

Combined U–Th and (U–Th)/He eruption ages were determined in replicate for zircon extracted from five lava samples and five single pumice clasts (Table 1; Fig. 2). The oldest eruption age is for quartz-poor pumice near Bellevue village (SL-JL-57) that overlies paleosol developed on top of an andesite block-and-ash-flow deposit. This pumice deposit has been previously mapped as Choiseul tuff (Wright et al., 1984; Wohletz et al., 1986), but is shown here to be significantly older than compositionally similar pumice from the Choiseul type locality (Lindsay 2005). Its eruption age (264 ± 8 ka; 1σ uncertainty; n = 9; Q = 0.56) overlaps within uncertainty with Morne Bonin lava (SL-JL-23: 273 ± 15 ka; n = 3; Q = 0.061). Quartz-poor pumice

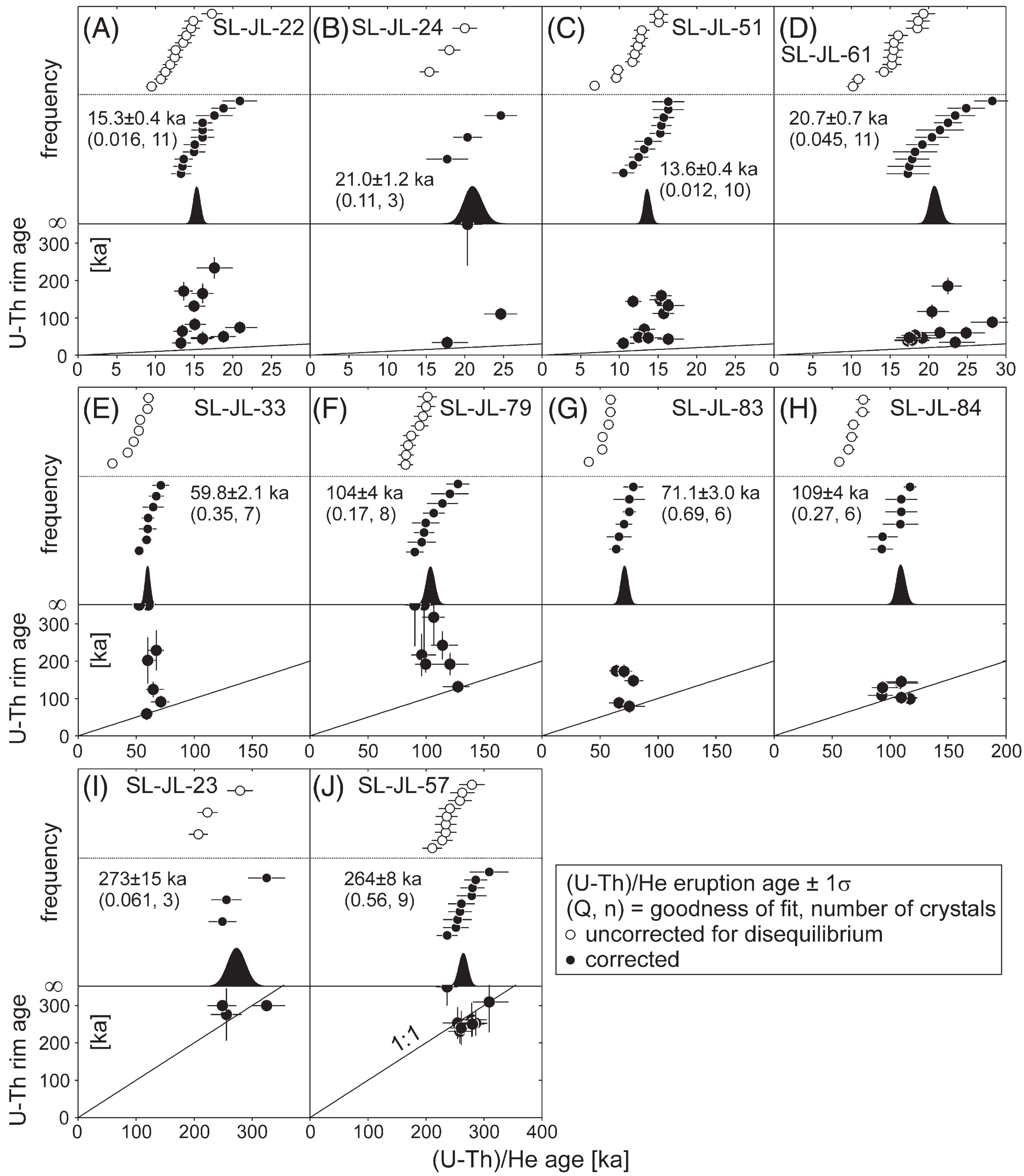

Fig. 2. Combined U–Th and (U–Th)/He zircon ages. Each panel shows the uncorrected ages (top), the disequilibrium-corrected ages, and a Gaussian fit to replicate analyses representing the modeled eruption age (middle). The lower panel compares corrected (U–Th)/He ages with the U–Th zircon rim crystallization ages. Ages below the 1:1 line are impossible because zircon crystallization must predate the eruption.

sampled near sea-level at the Anse John location (SL-JL-79: 104 ± 4 ka; $n = 8$; $Q = 0.17$) is also significantly older than stratigraphically equivalent Choiseul tuff (Lindsay, 2005). Its age, however, overlaps with that for Petit Piton lava (SL-JL-84: 109 ± 4 ka; $n = 6$; $Q = 0.27$). Gros Piton lava yields a significantly younger eruption age (SL-JL-83: 71.1 ± 3.0 ka; $n = 6$; $Q = 0.69$). The younger age for pumice sampled ~24 m above sea-level at La Pointe beach (SL-JL-33: 59.8 ± 2.1 ka; $n = 7$; 0.35) is stratigraphically consistent with the older age for SL-JL-79. Two samples of Belfond pumice were collected from the base and near the top of a ~30 m tuff section at Migny. They yield overlapping ages of 21.0 ± 1.2 ka (SL-JL-24: $n = 3$; $Q = 0.11$) and 20.7 ± 0.7 ka (SL-JL-61: $n = 11$; $Q = 0.045$). These Belfond pyroclastic flow deposits represent the youngest dated explosive eruptions. Two morphologically young lava domes yield slightly younger ages, overlapping within 2σ uncertainties (Belfond SL-JL-51: 13.6 ± 0.4 ka; $n = 10$; $Q = 0.012$ and Terre Blanche SL-JL-22: 15.3 ± 0.4 ka; $n = 11$; $Q = 0.016$).

3.2. Zircon crystallization ages

In contrast to (U–Th)/He ages which are homogeneous for individual samples, U–Pb and U–Th crystallization age distributions are complex (Figs. 3–5). This reflects the fact that parent and daughter isotopes in the U–Th–Pb decay systems (with the exception of ^{4}He) are essentially immobile in zircon even at magmatic temperatures (Cherniak and Watson, 2003), and therefore preserve pre-eruptive

Table 1
U–Th and (U–Th)/He zircon results for the Soufrière Volcanic Center. Eruption ages are based on MCHeCalc calculations producing the best fit for different estimates of the crystallization age (rim, average interior, or equilibrium).

Zircon	(^{238}U)/(^{232}Th)		(^{230}Th)/(^{232}Th)		U–Th age (ka)			U (ppm)	Th (ppm)	D230	He (nmol/g)	Ft	Equilibrium (U–Th)/He age (ka)		Disequilibrium (U–Th)/He age (ka)			Remarks
		±		±		+	−							±		+	−	
SL-JL-22 lava boulder from E slope of Terre Blanche dome (N13°50′39.5″ W61°02′07.1″)																		
(U–Th)/He age 15.3 ka (+0.43, −0.42 ka), $n=11$, goodness-of-fit = 0.016																		
z1	19.85	0.51	8.419	0.625	55.0	6.4	−6.1	141	34.1	0.06	0.0104	0.87	14.9	1.2	16.1	1.4	1.4	a
z1-r	18.56	0.41	7.502	0.603	51.0	6.3	−5.9	"	"	"	"	"	"	"	"	"	"	
z1-r	19.46	0.41	6.955	0.665	43.1	6.1	−5.7	"	"	"	"	"	"	"	"	"	"	
z3	9.594	0.129	2.749	0.163	26.3	2.9	−2.8	335	88.9	0.06	0.0216	0.85	12.5	1.0	13.5	1.2	1.2	a
z7	26.32	0.44	23.44	0.71	234	34	−26	183	38.7	0.05	0.0129	0.86	14.6	1.2	16.1	1.2	1.5	
z2	27.64	1.01	15.11	0.74	82.4	8.2	−7.6	347	66.1	0.04	0.0269	0.80	17.3	1.4	18.8	1.6	1.7	a
z4	11.35	0.20	4.634	0.241	48.0	4.2	−4.1	321	74.1	0.05	0.0187	0.82	12.6	1.0	13.6	1.2	1.2	a
z4-r	11.64	0.28	4.610	0.268	46.1	4.6	−4.4	"	"	"	"	"	"	"	"	"	"	
z5	10.40	0.15	4.121	0.261	45.1	4.8	−4.6	442	81.2	0.04	0.0293	0.84	14.0	1.1	15.1	1.5	1.3	a
z5-r	10.88	0.22	4.157	0.286	43.0	4.9	−4.7	"	"	"	"	"	"	"	"	"	"	
z5-r	10.82	0.18	4.272	0.276	45.2	4.9	−4.7	"	"	"	"	"	"	"	"	"	"	
z6	10.48	0.17	3.381	0.165	32.8	2.8	−2.8	291	67.2	0.05	0.0134	0.86	9.5	0.8	20.9	2.3	1.9	
z8	32.38	1.79	25.92	0.45	171	28	−22	249	32.4	0.03	0.0138	0.88	11.3	0.9	13.3	1.3	1.2	
z9	14.63	0.44	7.043	1.241	64.3	19.4	−16.5	170	36.9	0.05	0.00859	0.83	10.7	0.9	17.6	2.4	2.3	
z30	15.10	0.38	5.444	0.291	42.0	3.7	−3.5	329	79.4	0.06	0.0209	0.82	13.6	1.1	16.1	1.5	1.5	
z32	9.020	0.189	2.969	0.183	32.2	3.6	−3.5	255	62.4	0.06	0.0144	0.84	11.9	0.9	15.0	1.5	1.2	
SL-JL-23 lava boulder from W slope of Morne Bonin dome (N13°49′45.7″ W61°01′51.3″)																		
(U–Th)/He age 273 ka (+15.4, −15.1 ka), $n=3$, goodness-of-fit = 0.061																		
z1	8.889	0.128	8.605	0.381	325	401	−74	167	49.3	0.07	0.1672	0.78	223	18	256	26	27	
z1-r	8.832	0.130	7.944	0.300	226	42	−30	"	"	"	"	"	"	"	"	"	"	
z2	25.90	0.75	25.78	1.08	505	∞	−201	253	75.3	0.07	0.3277	0.81	279	22	325	32	26	
z2-r	26.79	0.88	26.31	0.61	409	∞	−109	"	"	"	"	"	"	"	"	"	"	
z3	9.378	0.074	2.930	0.447	30	7.8	−7.3	153	41.1	0.06	0.1560	0.83	207	17	249	24	26	
z3-r	9.468	0.136	3.370	1.321	37.1	26.1	−21	"	"	"	"	"	"	"	"	"	"	
SL-JL-24 pumice clast from base of pyroclastic flow deposit near Migny (N13°50′15.1″ W61°01′09.9″)																		
(U–Th)/He age 21.0 ka (+1.2, −1.1 ka), $n=3$, goodness-of-fit = 0.11																		
z1	10.99	0.09	8.019	0.403	131	16	−14	172	47.6	0.06	0.0144	0.81	18.0	1.4	24.7	2.1	2.2	
z1-r	11.77	0.21	7.654	0.264	104	8	−7	"	"	"	"	"	"	"	"	"	"	
z2	25.90	0.75	25.78	1.08	505	∞	−201	553	114	0.05	0.0512	0.82	20.0	1.6	20.4	1.9	1.6	
z2-r	26.79	0.88	26.31	0.61	409	∞	−109	"	"	"	"	"	"	"	"	"	"	
z3	9.378	0.074	2.930	0.447	30.0	7.8	−7.3	419	101	0.06	0.0306	0.83	15.4	1.2	17.7	2.7	2.0	b
z3-r	9.468	0.136	3.370	1.321	37.1	26.1	−21	"	"	"	"	"	"	"	"	"	"	
SL-JL-33 pumice clast below ash layer 24 m a. s. l. (N13°47′17.3″ W61°03′47.95″)																		
(U–Th)/He age 59.8 ka (+2.1, −2.1 ka), $n=7$, goodness-of-fit = 0.35																		
z2	14.94	0.13	6.765	0.317	58.7	4.4	−4.2	135	33.9	0.06	0.0194	0.86	29.5	2.4	59.0	4.0	5.3	
z3	10.03	0.11	8.707	0.821	202	92	−49	141	37.0	0.06	0.0370	0.86	53.4	4.3	59.9	7.6	5.4	
z11	20.11	0.63	20.37	0.79	∞	∞	∞	483	75.6	0.04	0.1365	0.84	60.6	4.8	60.2	5.2	4.4	
z15	11.85	0.53	12.23	0.70	∞	∞	∞	105	27.5	0.06	0.0258	0.82	52.3	4.2	52.5	4.1	4.4	
z18	11.31	0.48	10.15	0.48	229	75	−44	126	34.8	0.06	0.0362	0.83	59.8	4.8	67.3	6.5	7.0	
z19	10.27	0.16	6.258	0.173	91.2	5.6	−5.3	198	58.3	0.07	0.0401	0.82	42.7	3.4	71.2	7.3	8.6	
z21	22.01	1.01	15.27	1.14	124	23	−19	263	94.3	0.08	0.0610	0.83	47.8	3.8	64.7	9.1	6.5	
SL-JL-51 lava from block-and-ash-flow deposit from Belfond Dome (N13°49′14.0″ W61°02′24.5″)																		
(U–Th)/He age 13.6 ka (+0.45, −0.39 ka), $n=10$, goodness-of-fit = 0.012																		
z2	10.32	0.15	5.358	0.157	69.2	4.1	−3.9	207	46.9	0.05	0.0121	0.86	12.0	1.0	13.2	1.4	1.4	c
z3	16.46	0.33	6.426	0.500	47.8	5.7	−5.4	404	90.3	0.05	0.0126	0.80	6.8	0.5	12.5	1.3	1.1	
z4	22.26	0.38	7.842	0.358	42.9	2.9	−2.9	377	92.9	0.06	0.0260	0.80	15.1	1.2	16.3	2.0	1.4	c
z7	19.06	0.31	5.435	0.337	31.4	2.8	−2.8	302	68.6	0.05	0.0144	0.86	9.8	0.8	10.5	1.4	0.9	c
z8	9.936	0.132	6.750	0.304	112	11	−10	254	68.5	0.06	0.0136	0.80	11.7	0.9	15.7	1.3	1.4	
z10	17.99	0.48	13.67	0.57	148	18	−16	215	35.5	0.04	0.0121	0.81	12.4	1.0	15.3	1.4	1.4	
z12	10.67	0.18	4.297	0.185	46.4	3.5	−3.4	279	67.0	0.06	0.0168	0.83	12.7	1.0	13.8	1.7	1.2	c
z13	9.757	0.325	7.462	0.256	144	17	−15	176	45.1	0.06	0.00783	0.81	9.6	0.8	11.8	1.1	1.0	
z14	9.653	0.108	7.702	0.293	159	18	−15	138	35.1	0.06	0.00833	0.82	12.9	1.0	15.4	1.3	1.4	
z15	11.19	0.10	8.202	0.345	132	13	−12	231	62.9	0.06	0.0152	0.76	15.1	1.2	16.3	2.1	1.5	c
SL-JL-57 pumice clast from pyroclastic flow deposit ca. 1.5 m above paleosoil, roadcut near Dugard (N13°48′06.1″ W61°02′12.8″)																		
(U–Th)/He age 264 ka (+7.7, −7.4 ka), $n=9$, goodness-of-fit = 0.56																		
z1	8.418	0.136	7.889	0.192	268	49	−34	231	72.6	0.07	0.1550	0.79	147	12	–	–	–	f
z2	11.65	0.34	11.95	0.46	∞	∞	∞	150	45.8	0.07	0.1630	0.80	236	19	237	18	19	
z6	7.996	0.111	7.468	0.248	262	59	−38	195	60.4	0.07	0.2183	0.83	234	19	279	26	26	a
z7	8.525	0.138	7.887	0.190	253	40	−29	305	112	0.09	0.3345	0.80	234	19	286	20	26	a
z9	8.658	0.183	8.326	0.293	310	150	−61	300	123	0.10	0.3909	0.79	279	22	309	33	28	

(continued on next page)

Table 1 (*continued*)

Zircon	(^{238}U)/(^{232}Th)	±	(^{230}Th)/(^{232}Th)	±	U–Th age (ka)	+	−	U (ppm)	Th (ppm)	D230	He (nmol/g)	Ft	Equilibrium (U–Th)/He age (ka)	±	Disequilibrium (U–Th)/He age (ka)	+	−	Remarks
SL-JL-57 pumice clast from pyroclastic flow deposit ca. 1.5 m above paleosoil, roadcut near Dugard (N13°48′06.1″ W61°02′12.8″)																		
(U–Th)/He age 264 ka (+7.7, −7.4 ka), $n=9$, goodness-of-fit = 0.56																		
z10	8.112	0.139	7.517	0.248	253	55	−36	279	73.6	0.06	0.2762	0.82	211	17	254	25	25	
z11	8.751	0.138	7.911	0.247	231	38	−28	195	51.7	0.06	0.2389	0.83	258	21	258	21	20	
z12	9.971	0.243	9.077	0.364	240	59	−38	163	44.6	0.06	0.2075	0.85	263	21	261	23	19	
z13	14.94	0.54	14.65	0.64	385	∞	−120	262	69.5	0.06	0.2893	0.80	241	19	252	22	23	
z15	8.528	0.111	7.869	0.205	250	39	−29	208	59.9	0.07	0.2320	0.85	228	18	280	21	25	
SL-JL-61 pumice clast from top of pyroclastic flow deposit near Migny (N13°50′15.1″ W61°01′09.9″)																		
(U–Th)/He age 20.7 ka (+0.7, −0.6 ka), $n=11$, goodness-of-fit = 0.045																		
z1	13.20	0.55	9.032	0.654	116	21	−18	340	86.1	0.06	0.0128	0.86	15.5	1.2	20.4	2.2	1.9	
z2	11.83	0.26	4.137	0.147	38.3	2.6	−2.5	396	126	0.07	0.0278	0.79	15.2	1.2	17.3	2.8	1.7	b
z4	20.98	0.32	9.476	0.505	60.6	5.1	−4.8	192	48.3	0.06	0.0170	0.84	18.5	1.5	21.5	3.1	2.5	b
z5	10.20	0.18	4.825	0.226	59.3	5	−4.8	274	71.1	0.06	0.0188	0.85	14.2	1.1	24.8	2.4	2.3	
z7	16.19	0.49	6.142	0.364	45.7	4.5	−4.3	426	112	0.06	0.0203	0.82	10.2	0.8	19.2	2.1	1.6	
z8	19.50	0.26	8.097	0.474	53.2	4.7	−4.5	229	53.7	0.05	0.0172	0.82	16.0	1.3	18.2	2.9	1.8	b
z9	13.32	0.21	11.13	0.42	185	24	−20	269	68.3	0.06	0.0244	0.82	19.3	1.5	22.5	1.8	2.1	
z11	18.49	0.25	10.70	0.48	88.1	7.1	−6.7	284	74.8	0.06	0.0245	0.81	18.6	1.5	28.2	2.4	2.8	
z12	11.46	0.42	4.184	0.255	40.6	4.4	−4.3	302	72.5	0.06	0.0219	0.83	15.3	1.2	17.9	2.2	2.3	b
z13	17.34	0.28	6.626	0.433	46.6	4.6	−4.4	290	70.2	0.06	0.0215	0.83	15.5	1.2	17.5	2.8	1.7	b
z15	9.696	0.101	3.256	0.136	34.1	2.6	−2.6	260	72.7	0.06	0.0136	0.84	10.9	0.9	23.4	2.6	2.1	
SL-JL-79 pumice clast from base of exposed flow deposit Anse John beach (N13°46′45.3″ W61°03′12.3″)																		
(U–Th)/He age 104 ka (+3.7, −3.5 ka), $n=8$, goodness-of-fit = 0.17																		
z1	9.930	0.135	7.296	0.247	131	11	−10	190	46.5	0.06	0.0736	0.83	82.3	6.6	127	10	13	
z2	11.42	0.55	10.08	0.60	216	80	−46	462	96.6	0.05	0.1780	0.81	84.6	6.8	96.3	12.2	9.1	
z4	9.491	0.117	7.093	0.226	136	11	−10	205	56.9	0.06	0.0411	0.81	43.0	3.4	–	–	–	f
z6	11.18	0.35	10.93	0.44	361	∞	−98	554	149	0.06	0.2359	0.79	94.5	7.6	98.3	8.8	8.8	
z8	20.28	0.52	19.94	0.51	407	∞	−101	453	70.0	0.04	0.1829	0.83	87.2	7.0	90.4	7.6	8.3	
z9	8.583	0.122	7.358	0.251	192	25	−20	206	61.0	0.07	0.0814	0.83	82.8	6.6	99.8	11.9	9.3	
z11	9.219	0.194	8.427	0.260	242	46	−32	227	58.4	0.06	0.1095	0.83	101	8	114	13	10	
z12	11.21	0.29	9.533	0.431	192	35	−27	273	43.1	0.04	0.1260	0.85	97.4	7.8	121	16	12	
z13	10.49	0.19	10.08	0.31	317	128	−57	228	56.4	0.06	0.1056	0.81	100	8	107	9	10	
z14	9.736	0.120	7.302	0.213	137	11	−10	271	73.1	0.06	0.0689	0.81	54.6	4.4	–	–	–	f
SL-JL-83 lava boulder from N slope of Gros Piton dome (N13°49′04.0″ W61°04′03.3″)																		
(U–Th)/He age 71.1 ka (+3.1, −3.0 ka), $n=6$, goodness-of-fit = 0.69																		
z2	13.08	0.37	10.70	0.22	174	18	−15	193	41.7	0.05	0.0544	0.89	56.2	4.5	78.8	8.6	7.7	
z3	10.36	0.19	5.847	0.173	79.7	5.1	−4.9	222	54.0	0.06	0.0834	0.86	76.3	6.1	64.0	6.1	6.0	
z5	17.53	0.29	9.436	0.356	78.0	5.3	−5.1	188	42.0	0.05	0.0583	0.85	64.2	5.1	66.3	10.9	8.6	d
z6	9.048	0.145	7.462	0.249	172	20	−17	326	76.2	0.05	0.1223	0.86	76.8	6.1	75.3	5.6	7.1	
z8	10.19	0.19	5.729	0.131	79.0	4.3	−4.2	83	22.2	0.06	0.0288	0.88	68.3	5.5	70.7	7.2	6.7	
z4	10.67	0.19	6.355	0.168	87.9	5.3	−5	272	60.4	0.05	0.0863	0.84	66.9	5.3	75.3	13.7	9.2	d
SL-JL-84 lava boulder from N slope of Petit Piton dome (N13°50′20.9″ W61°03′52.6″)																		
(U–Th)/He age 109 ka (+4.0, −3.4 ka), $n=6$, goodness-of-fit = 0.27																		
z1	11.14	0.26	8.074	0.255	129	11	−10	153	35.7	0.05	0.0445	0.86	59.2	4.7	92.8	9.7	12.0	
z2	10.31	0.16	6.900	0.185	109	7	−7	186	42.9	0.05	0.0473	0.86	52.3	4.2	109	15	11	
z4	10.69	0.22	6.894	0.186	102	7	−6	277	68.0	0.06	0.0705	0.86	51.9	4.2	93.6	12.9	9.3	
z5	10.01	0.22	7.297	0.190	129	10	−9	288	67.1	0.05	0.0567	0.86	40.3	3.2	110	14	13	
z6	11.43	0.38	8.727	0.251	145	16	−14	227	59.9	0.06	0.0623	0.84	57.4	4.6	117	6	6	
z8	10.54	0.21	6.708	0.147	99.0	5.9	−5.6	355	59.7	0.04	0.0999	0.85	59.0	4.7	110	14	6	

All errors 1σ.
∞ secular equilibrium; n.a. = not analyzed; * = no correction applied because grain is in secular equilibrium.
U–Th age from slope through zircon and whole-rock (Turner et al., 1996) composition.
Parentheses denote activities; D230 = [232Th/238U]zircon/[232Th/238U]whole-rock; Ft = alpha particle ejection correction parameter.
Decay constants used: λ(230Th): $9.1577 \cdot 10^{-6}$ a^{-1}; λ(232Th): $4.9475 \cdot 10^{-11}$ a^{-1}; λ(238U): $1.55125 \cdot 10^{-10}$ a^{-1}; λ(226Ra) = $4.332 \cdot 10^{-4}$ a^{-1}.
Zircon U-series analyses by ion microprobe.
Zircon(U–Th)/He analysis by inductively coupled mass spectrometry (U, Th), and quadrupole mass spectrometry (He).
Remarks: when rim ages resulted in eruption age > crystallization age, disequilibrium correction was based on average interior ages: a = secular equilibrium; b = 131 ± 95 ka; c = 178 ± 127 ka; d = 127 ± 54 ka; and f = incomplete degassing during laser heating (excluded).

crystallization ages. Overall, 413 U–Th and 37 U–Pb zircon ages were determined on 385 individual crystals. The key observations regarding the zircon crystallization ages are:

(1) SVC zircon ages are entirely Late Pleistocene (Fig. 3 and Supplementary data), with the oldest U–Pb zircon ages at ~600 ka;
(2) Rim ages are on average younger than interior ages, although significant overlap exists (Fig. 3);
(3) Continuous depth profiling reveals that zircon crystals are age-zoned (Fig. 4) and that rim and core ages differ by ~200–300 ka. Fig. 4 also illustrates that the ion microprobe spot can overlap different age domains and produce mixed ages for

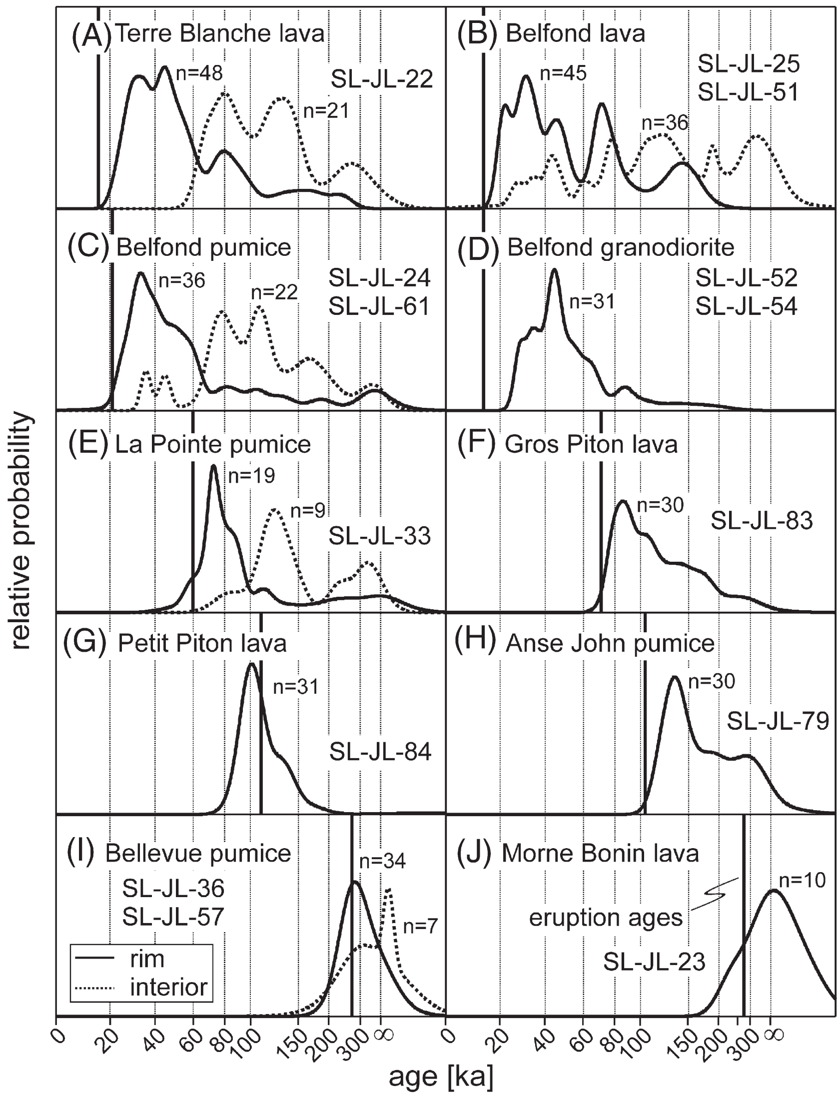

Fig. 3. Distributions of U–Th zircon model ages derived from two-point isochrons through whole-rock (Turner et al., 1996) and zircon (Supplementary data). For sample populations comprising >30 crystals, any age population present at >10% of the overall population should have been detected at 95% confidence (Dodson et al., 1988). Thick vertical line indicates disequilibrium-corrected (U–Th)/He zircon eruption age. Selected zircon crystals within error of secular equilibrium were also dated by U–Pb methods, and generally found to be <600 ka (Supplementary data).

conventionally sectioned crystals. Depth profiling rim analyses are therefore generally considered more reliable;

(4) Cathodoluminescence images (CL) of sectioned crystals may (Fig. 4B) or may not (Fig. 4A) show age domains that were detected in continuous depth profiling analysis;

(5) The youngest rim ages overlap within uncertainty with the (U–Th)/He eruption ages (Fig. 3), but many zircon crystals have rim ages significantly older than the eruption;

(6) Granodiorite inclusions (SL-JL-52 and -54) show variable zircon rim ages ranging between ~30 ka and ~180 ka, similar to those in their host lavas (Fig. 3);

(7) Rim and interior age distributions are polymodal (Fig. 3), with overlapping peaks in the distributions at ~35, ~45, ~80, and ~130 ka. Older age modes are present, but are less precisely resolved as radioactive equilibrium is approached and age uncertainties increase. It also appears that zircon age distributions become progressively more complex in younger units, although this is biased by the higher absolute dating precision of the U–Th method for younger crystals, and our emphasis on analyzing mostly zircon rims for the older units. A detailed analysis of these age distributions is presented in the next section.

3.3. Magmato-detrital zircon age spectrum analysis

Polymodal U–Th zircon age distributions have been previously reported for young volcanic rocks, but interpretation of age modes remained qualitative (e.g., Wilson and Charlier, 2009). Here, we apply Kolmogorov–Smirnov (KS) statistical analysis (Press et al., 1988) that also has been employed for sedimentary detrital zircon (Fletcher et al., 2007) to quantitatively compare age distributions among individual and composite samples.

A basic test of the KS approach is to compare U–Th zircon crystallization age distributions of two samples of Belfond lava (both rim and interior analyses; Fig. 5A). This test yields an acceptably high probability for both samples having identical zircon populations (probability of equivalency $P=0.27$), whereby the hypothesis that populations are identical is rejected when $P<0.05$ (Press et al., 1988). It also indicates that sampling sizes (>30 analyses) are statistically representative. Next, we compare Belfond lava dome zircon ages (rim

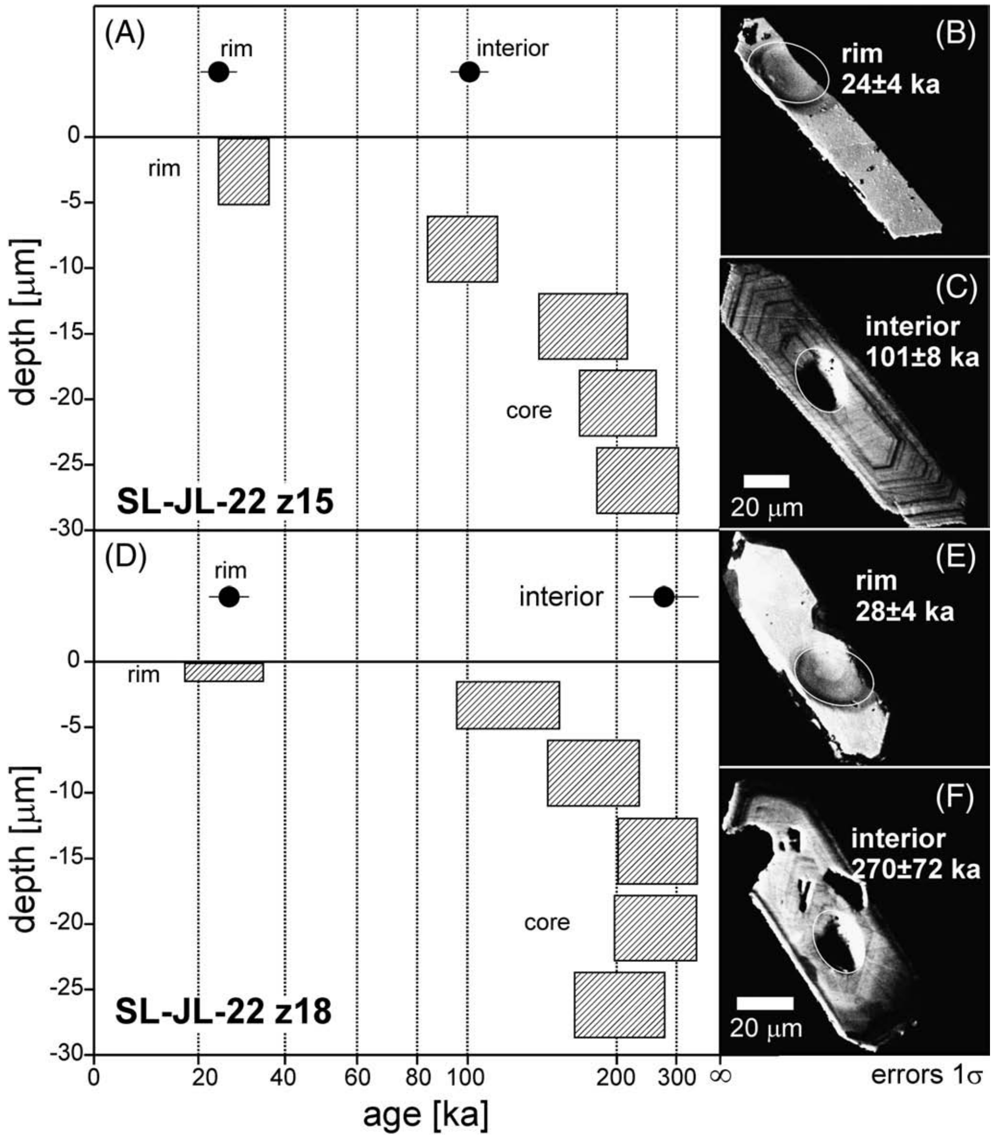

Fig. 4. U–Th zircon spot analyses (rims and interiors) and depth profiling ages for Terre Blanche zircon crystals SL-JL-22 z15 (A–C) and z18 (D–F). Crystals were initially analyzed as "rims" on original crystal surfaces, and then sectioned to ~2/3 of their original thickness. The sectioned crystals were then remounted in order to expose the opposite crystal face which was depth profiled to ~28 μm (approximately half-way into the crystal). Depth vs. age plots integrating multiple analysis cycles (boxes) show excellent reproducibility of the depth profiling core ages with the interior spot analysis for grain z18, whereas the younger interior spot age in z15 results from beam overlap onto younger rims detected between 0 and 10 μm in depth profiling. B and E show CL images of original crystal surfaces, whereas C and F are CL images of the same crystals after sectioning. Note that the boundaries of the age domains in z15 are not readily distinguished in the CL images showing oscillatory zonation typical for igneous zircon without discontinuities or truncations of CL bands. Crater depths were determined using a contact-free surface mapper, translating into sputtering rates of ~0.001 μm/s.

and interiors) with those of Belfond pumice, and find them equivalent at high probability ($P = 0.997$; Fig. 5B). Moreover, zircon rim ages of Belfond lava are indistinguishable from those of granodiorite inclusions that erupted with these lavas (probability $P = 0.55$; Fig. 5C). In contrast, little overlap exists between zircon rims and interiors from a composite distribution of both young lava domes (Terre Blanche and Belfond) ($P = 0.4 \times 10^{-9}$; Fig. 5D). The zircon interior age distribution from the young lava domes, however, agrees closely with the composite U–Th zircon crystallization age distribution from all SVC precursor eruptions ranging in age between ~20 (Belfond tuff) and ~270 ka (Morne Bonin and Bellevue) ($P = 0.985$; Fig. 5E).

It is possible that the composite SVC zircon age distribution in Fig. 5E is biased due to incomplete sampling. From stratigraphic relations, however, we are confident that we have included the oldest SVC pyroclastic deposits because they directly overlie paleosol and andesitic block-and-ash-flow deposits that predate the Qualibou depression. Despite the possibility of missing some potential eruptions of intermediate age, it is important to note that a significant zircon population with ages between ~70 and 150 ka exists in zircon interiors from young domes located in the central part of the depression. This population is characteristic for zircon from lavas of the Petit and Gros Pitons from the western margin of the Qualibou depression, despite the absence of lavas with such ages in the center of the depression.

4. Discussion

4.1. Duration of zircon crystallization by combined U–Th and (U–Th)/He zircon dating and depth profiling

By using combined U–Th and (U–Th)/He zircon dating, we effectively circumvent the problem that K–Ar (including Ar–Ar) dating methods frequently yield apparent eruption ages that are older than U–Th zircon ages (e.g., Claiborne et al., 2009). These inconsistencies are likely due to excess ^{40}Ar (as was demonstrated for

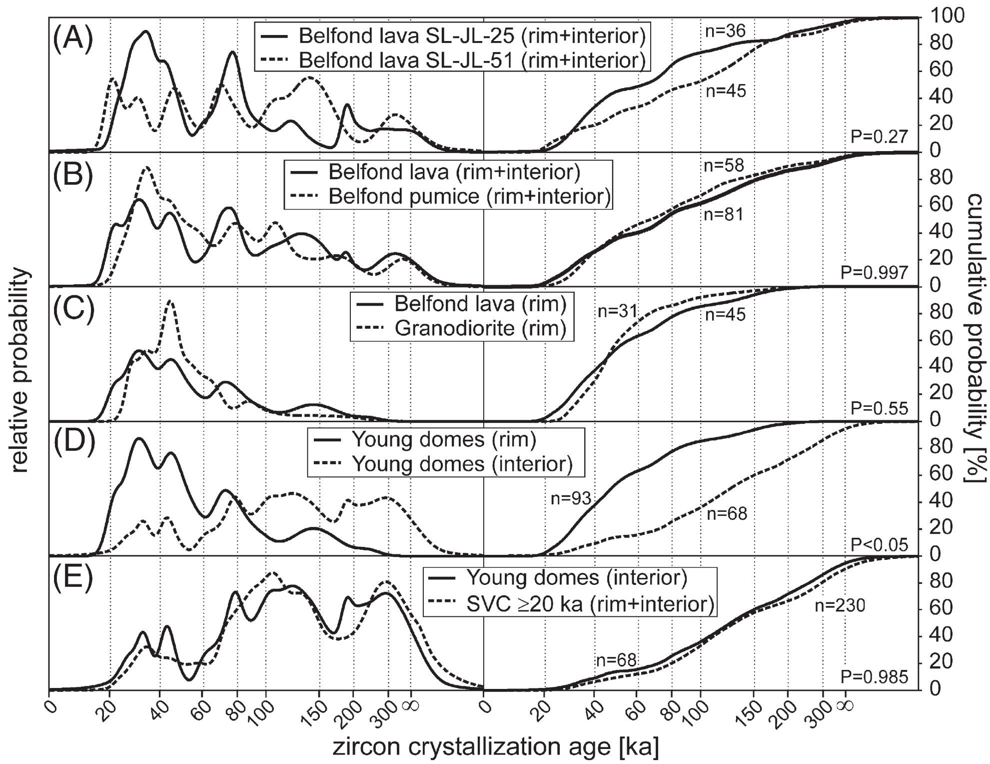

Fig. 5. Zircon crystallization age probability density curves showing results of Kolmogorov–Smirnov statistical comparison between age populations. Probabilities $P>0.05$ indicate that the populations being compared are indistinguishable at the 95% confidence level (Press et al., 1988). Curves comprise the following samples: (A) individual curves for SL-JL-25 and SL-JL-51; (B) Belfond lava (SL-JL-25 and -51) and Belfond pumice (SL-JL-24 and -61); (C) Belfond lava (SL-JL-25 and -51) and granodiorite (SL-JL-52 and -54); (D) young domes (SL-JL-22, -25, and -51); (E) young domes interior (SL-JL-22, -25, and -51) and SVC ≥20 ka (SL-JL-23, -24, -33, -36, -57, -61, -75, -79, -83, -84).

plagioclase from SVC lavas by Samper et al., 2008). We find excellent agreement between combined U–Th and (U–Th)/He ages and ^{14}C charcoal ages for Belfond pyroclastic deposits, but could not confirm ^{14}C ages around 30–40 ka (near the limit of ^{14}C geochronology) for the Choiseul deposit (Lindsay, 2005). Our results indicate that quartz-poor pumice deposits collectively mapped as Choiseul tuff include at least two eruptions at 104 ka and 264 ka. Unspiked groundmass K–Ar and disequilibrium-corrected (U–Th)/He ages overlap for Gros Piton lava (within 2σ limits), whereas those for Terre Blanche and Petit Piton disagree (Fig. 6). Resetting of zircon by later thermal events can be ruled out because the K–Ar ages are younger than the zircon ages. With regard to Terre Blanche, we emphasize that care was taken to collect a sample from the eastern flank of the dome, away from the presently active Sulphur Springs geothermal system.

The observation that the youngest mode in the U–Th zircon age distribution closely overlaps with the disequilibrium-corrected (U–Th)/He zircon ages suggests that some zircon crystallized immediately prior to eruption. This independently, but not conclusively, supports the accuracy of the (U–Th)/He eruption ages. We can, however, confidently rule out significant overcorrection of the (U–Th)/He ages which would otherwise violate the constraint that eruption must postdate crystallization, i.e., ages must plot above the 1:1 line in the U–Th rim vs. (U–Th)/He age diagram (Fig. 2). The vertical trends in these plots (Fig. 2) reveal that zircon rim crystallization often significantly (by 10 s to 100 s of ka) predates the eruption.

4.2. Zircon crystallization lacunae: subsolidus crystal residence?

Our U–Th zircon depth profiling approach minimizes potential artifacts that can result from beam overlap onto different age domains in sectioned crystals which could produce mixed ages of debatable geological significance (e.g., Fig. 4B). Depth profiling reveals that individual SVC zircon crystals are zoned in age: rims ~2–5 µm thick (corresponding to ~10–30% of the zircon volume assuming spherical geometry and a 50 µm crystal radius) crystallized ~100–300 ka after the interiors. Whereas some zircon rims crystallized near the eruption, crystal interiors (analyzed by depth profiling, or on sectioned crystals) almost exclusively predate the eruption by 10 s to 100 s of ka, consistent with previous results for silicic volcanic systems (e.g. Reid et al., 1997; Simon et al., 2008). Notably, the transition between age domains only sometimes correlates with CL visible boundaries (Fig. 4B), whereas other crystals show significant age transitions without obvious breaks in oscillatory CL patterns (Fig. 4A). This cautions against interpretation of CL patterns that lack apparent discontinuities as representing a simple crystallization history. Within the resolution of ion microprobe U–Th depth profiling (~1 µm), age transitions appear to be sharp, although the temporal resolution diminishes as core ages approach secular equilibrium.

Pronounced age gaps are inconsistent with protracted crystal residence in a partially molten crystal mush for which continuous (albeit at a reduced rate) zircon crystallization is predicted upon cooling (e.g., Harrison et al., 2007). Isothermal storage would seem fortuitous for the protracted time periods represented by zircon age gaps, and is inconsistent with the presence of granodiorite inclusions that indicate that at least some parts of the magma system cooled rapidly to subsolidus temperatures. This leaves the possibilities that zircon crystals were either discontinuously exposed to a melt phase, or became resorbed when the melt was intermittently undersaturated in zircon (e.g., due to heating and/or changes in melt composition). Resorption seems unlikely because zircon is ubiquitous in most SVC rocks throughout its entire history, which implies that SVC magmas were zircon-saturated. Moreover, resorption textures (rounded or truncated interior domains) are absent in crystals with pronounced age gaps (Fig. 4).

A second line of evidence is the scarcity of young (near-eruption) zircon rims. It is conceivable that crystals were shielded from the melt as

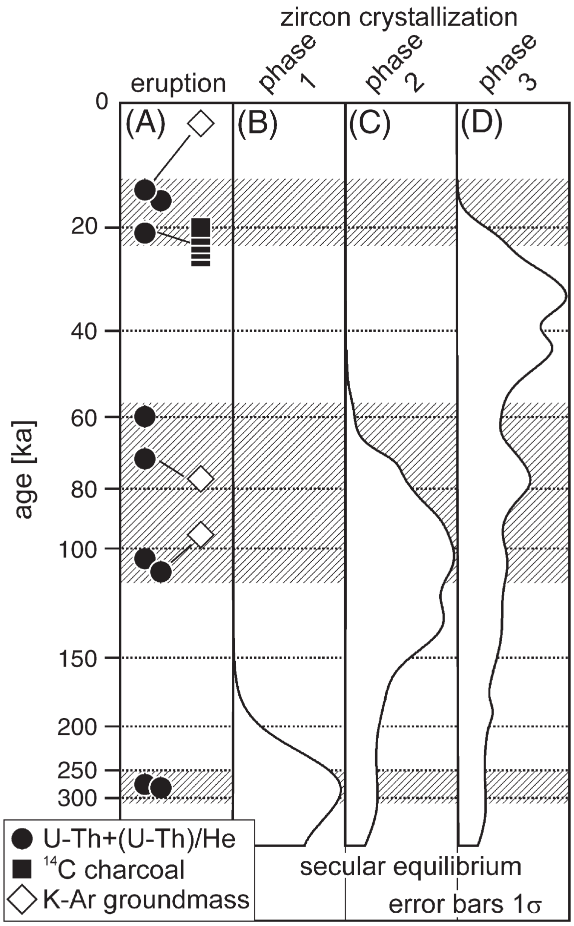

Fig. 6. Eruption age summary for the SVC in comparison to U–Th zircon crystallization ages. Tie-lines indicate excellent agreement between combined U–Th and (U–Th)/He eruption ages (this study) and published ^{14}C charcoal ages for Belfond tuff (Lindsay, 2005), whereas unspiked K–Ar ages deviate to younger or older ages (Samper et al., 2008). SVC eruption phases 1–3 are based on new (U–Th)/He results. For each phase, a significant gap exists between the onset of zircon crystallization and the earliest eruption.

inclusions in phenocrysts. If zircon crystals were indeed inclusions in other phases, the presence of glass adherent to the volcanic zircon requires that they would have been liberated from their host prior to eruption. Alternatively, near-eruption crystallization could have been kinetically inhibited. This could be the case if zircon crystals were scavenged from older rocks en route to the surface during the eruption. The lack of zircon with near-eruption ages in plutonic inclusions, however, cannot be explained by eruptive entrainment of crystals. Moreover, these inclusions have widely varying zircon rim ages, and their age distribution is indistinguishable from those of the lavas. We therefore strongly favor the interpretation that discontinuous contact between zircon and melt is due to intermittent storage under subsolidus conditions, and that zircon crystals from different parts of the plutonic complex became subsequently recycled and mixed. This scenario does not rule out a long-lived partially molten zone at depth, but at least for the portion of the magma system where zircon crystallized, we find little evidence for continuous presence of melt. Periodicity in both zircon crystallization and eruptive activity raises the question of whether there is a systematic relationship between them.

4.3. Episodic zircon crystallization and eruptive phases in the Soufrière Volcanic Complex

Figs. 6 and 7 summarize a modified evolutionary model for the SVC that integrates new evidence from U–Th and (U–Th)/He geochronology. We identify three major phases in the history of the SVC (Fig. 6): Phase 1 comprises early dacitic pyroclastic deposits and domes (Bellevue, Morne Bonin) erupted between ~290–270 ka. It is conceivable that phase 1 explosive activity triggered the collapse of the Qualibou depression as envisaged by Wohletz et al. (1986), but instead of a single "caldera-forming" eruption of the Choiseul tuff, we have identified at least two quartz-poor pyroclastic flow deposits with widely separated eruption ages. We assign the younger quartz-poor pumice tuff, informally named Anse John tuff (104 ka), to phase 2 eruptions, together with the eroded domes of Gros and Petit Piton (109 ka and 71 ka), and a previously undated quartz-rich pyroclastic flow deposit from the La Pointe beach location (60 ka). The most recent activity (phase 3) initiates with the eruption of Belfond tuff at ~20 ka, and also comprises the compositionally similar lava domes of Belfond and Terre Blanche. Our (U–Th)/He results provide no evidence for a Holocene eruption of Terre Blanche (cf. Samper et al., 2008). The causes for this discrepancy warrant further investigation.

The cumulative zircon age distributions for each eruptive phase are plotted in Fig. 6. For the youngest phase 3, zircon crystallization predates volcanism by about 10–20 ka (Fig. 6). This age difference is less obvious for the older phases due to the lower precision of U–Th ages near secular equilibrium. Nevertheless, the onset of zircon crystallization during phase 2 dates back to ~40 ka prior to the earliest eruptions. There is also evidence from U–Pb zircon dating that crystal interiors predate the eruption of phase 1 lavas and pyroclastic deposits by as much as ~300 ka.

A possible interpretation of the apparent decoupling between zircon crystallization and eruption is renewed intrusion of mantle-derived zircon-undersaturated magma. This recharge may have triggered the eruption of resident silicic magma from the previous phase (e.g., Eichelberger et al., 2000). In this interpretation, massive zircon crystallization would then initiate after a lag period that is required for cooling and differentiation of the newly arrived magma. Such a scenario of retrograde (upon magma cooling) zircon crystallization, however, does not readily explain why crystallization of zircon rims has largely ceased by the time of the next eruptive cycle.

We therefore propose an alternative view in which pulses of zircon crystallization are related to thermal rejuvenation of a subsolidus intrusive complex that caused remelting of earlier solidified intrusions. In this scenario, zircon crystallization occurs following an initially prograde heating path. The lag time between zircon crystallization and eruption could indicate the duration over which sufficient melt mobilization and accumulation had occurred to permit eruption. The absence of young zircon rims in some crystals suggests a non-uniform thermal history within the intrusive complex upon reheating, with some crystals being still heated up, and others already cooling (and crystallizing new zircon). It is also possible that renewed zircon crystallization is kinetically inhibited during the prograde path of partially melting a shallow pluton by low temperatures, and possibly low H_2O contents.

4.4. Magmatic zircon provenance and implications for arc crustal growth

Zircon interiors in young lava domes from the SVC provide a remarkably faithful record of earlier crystallization events, as indicated by their close match with the age distributions of granodiorite and cumulative older (≥20 ka) zircon ages. Similarities in zircon age distributions between cogenetic plutonic and volcanic rocks have been noted previously, for example for the Geysers–Cobb Mountain association (California Coast Ranges) (Schmitt et al., 2003a,b) or for plutonic enclaves and lavas from Crater Lake (Oregon) (Bacon and Lowenstern, 2005). In both cases, zircon recycling has been advocated whereby the erupted magma contained a large component of assimilated or remelted young plutonic rocks. The SVC zircon record supports a similar scenario based on two lines of evidence: (1) zircon crystallization age distributions are indistinguishable between plutonic

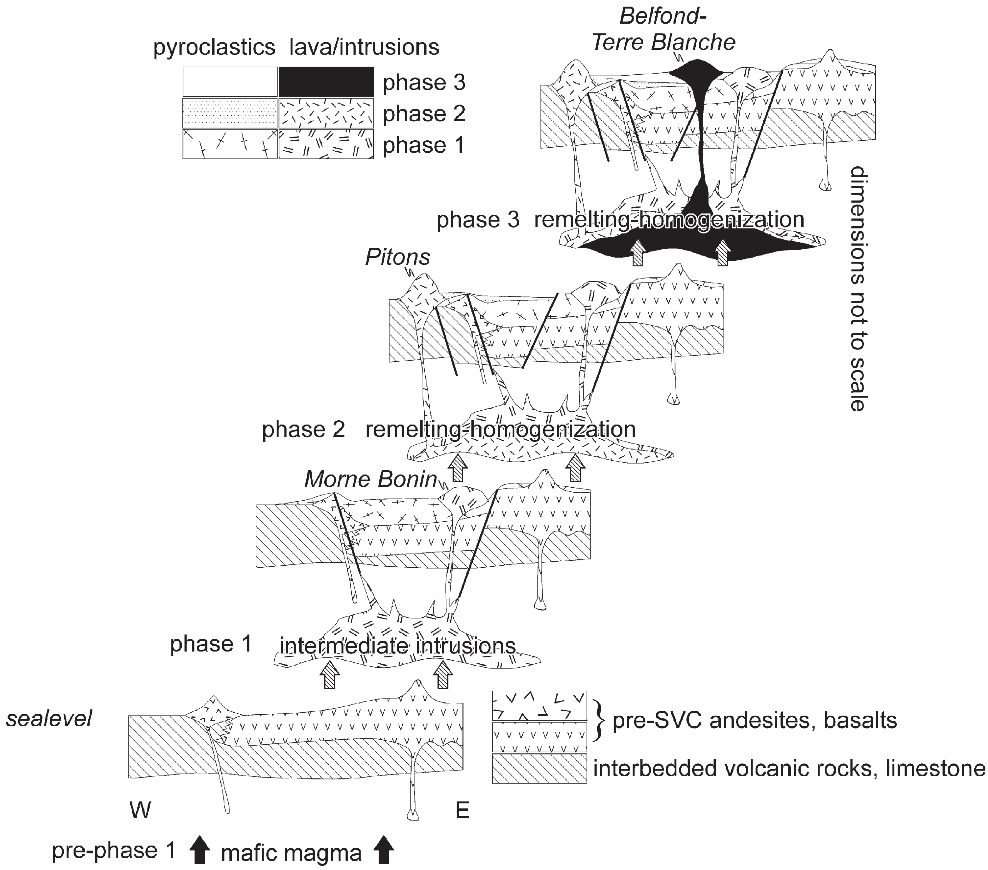

Fig. 7. Schematic model showing the major phases in the evolution of the SVC modified after Wohletz et al. (1986). Dark arrows indicate mafic magma input, hatched arrows addition of heat and/or differentiated magma. Based on closely overlapping zircon age populations in spatially separated lava domes, we envisage an integrated plutonic complex forming underneath the Qualibou depression, rather than separated magma batches feeding individual eruptions, or widespread Late Pleistocene pyroclastic deposits being sourced in the central highlands (cf. Wright et al., 1984).

inclusions and their host lava, and (2) the cumulative zircon age distribution of earlier volcanic episodes matches that of zircon interiors in young lavas.

Compared to previous studies, it is a new aspect of the SVC that it comprises eruptions from multiple spatially separated vents over a nearly 300 ka period. Lava domes located in different parts of the Qualibou depression have zircon age distributions that share characteristic age modes: for example, ages between ~70 and ~150 ka exist in Terre Blanche and Belfond domes, although no eruptions of this age are known from this part of the Qualibou depression, whereas zircon crystals with such ages dominate the Piton lavas at the western margin of the depression. Another similarity between zircon age populations from distant sources is the fact that near secular equilibrium crystals are present in both the Pitons and the Terre Blanche–Belfond domes, despite their spatial separation. Fig. 5 demonstrates these similarities not only qualitatively, but through quantitative analysis of the zircon age spectra. This allows fingerprinting of magmatic sources, in much the same way as detrital zircon traces sedimentary provenance. Common zircon age populations in SVC volcanic rocks therefore provide strong evidence for a large integrated plutonic complex underneath the Qualibou depression, rather than multiple small, isolated intrusions (Fig. 7). Zircon age fingerprinting also resolves a long-standing ambiguity by demonstrating that extensive SVC pyroclastic deposits in southern Saint Lucia are correlated with lava domes inside the Qualibou depression, and therefore likely originated from sources within the Qualibou depression and not from putative vents in the central highlands.

What remains paradoxical is that amalgamation of individual intrusions into a homogeneous pluton occurs despite some portion of the magma system being at near-solidus conditions where it appears to undergo episodic solidification and remelting. Seismic crustal and magma densities place the roots for Lesser Antilles volcanism at the interface between dense mafic oceanic crust and a complex of mid-crustal intrusions of intermediate composition which acts as a density filter that causes primitive basaltic magmas to become neutrally buoyant (Devine, 1995). Thermal models suggest that heat could be supplied to the evolving plutonic complex through mafic underplating (e.g., Annen, 2009), through percolation of high temperature exsolved gas from solidifying hydrous mafic magma underneath (Bachmann and Bergantz, 2006), or a combination thereof.

We propose episodic remelting within a complex of mid-crustal plutons of intermediate composition to explain discontinuous zircon crystallization episodes recorded in volcanic and plutonic zircon from the SVC. Because the mechanisms of thermal and mechanical reprocessing of the SVC plutonic roots remain obscure, it is impossible to exactly quantify the amounts of new input vs. recycled materials in erupted magmas. The compositional similarity and identical zircon age spectra of young dacitic lavas and co-erupted granodiorite inclusions, however, are permissive of whole-sale remelting of plutons. This implies that material and thermal inputs during magma recharge are largely decoupled, and that intermediate and silicic magmas only indirectly reflect upon accretion of new crust in mature island arcs.

5. Conclusions

We introduce the spectral analysis of zircon crystallization age distributions in order to fingerprint crystal provenance in a long-lived calc-alkaline arc volcanic complex. Combined U–Th and (U–Th)/He zircon geochronology establishes a new chronostratigraphic framework for the SVC with three major phases for eruption of compositionally similar dacitic magma at ~270 ka, ~110–60 ka, and ~21–14 ka. Zircon crystallization age distributions of temporally and spatially separated lavas from the SVC share characteristic similarities, and are indistinguishable from those of pyroclastic deposits in the vicinity of the SVC.

Individual zircon crystals frequently record multiple growth episodes over 10s to 100s ka timescales, and this age information is lost or inaccessible by bulk analysis methods. Sharp separation between age domains in individual zircon crystals, and polymodal age distributions at hand-sample scales revealed by SIMS analysis indicate that zircon crystallization was discontinuous. We interpret lacunae in the zircon crystallization record as caused by subsolidus crystal residence. This is supported by the presence of young granodiorite inclusions. We therefore postulate that the Qualibou depression in southern Saint Lucia is underlain by an integrated plutonic complex that amalgamated from individual magmatic pulses, and became recycled in subsequent volcanic episodes over a ~300 ka period. Intermediate magmas are a significant component in the volcanic compositional spectrum in mature island arc systems such as the Lesser Antilles. These magmas may not represent a direct progeny of mafic magma input, but rather thermally and mechanically reprocessed unerupted magma from earlier magmatic episodes.

Acknowledgements

Sara Freeman, Michelle Hopkins, and Tracy Howe are thanked for their assistance in mineral separation and sample preparation. We thank reviewers Olivier Bachmann and Calvin Miller, and journal editor Richard Carlson. This work was supported by the National Geographic Society grant 8517-08. The ion microprobe facility at UCLA is partly supported by a grant from the Instrumentation and Facilities Program, Division of Earth Sciences, National Science Foundation. JML is supported by a fellowship from the New Zealand Earthquake Commission.

Appendix A. Supplementary data

Supplementary data associated with this article can be found, in the online version, at doi:10.1016/j.epsl.2010.03.028.

References

Annen, C., 2009. From plutons to magma chambers: thermal constraints on the accumulation of eruptible silicic magma in the upper crust. Earth Planet. Sci. Lett. 284 (3–4), 409–416.

Arculus, R.J., Wills, K.J.A., 1980. The petrology of plutonic blocks and inclusions from the Lesser Antilles Island Arc. J. Petrology 21 (4), 743–799.

Bachmann, O., Bergantz, G.W., 2006. Gas percolation in upper-crustal silicic crystal mushes as a mechanism for upward heat advection and rejuvenation of near-solidus magma bodies. J. Volcanol. Geoth. Res. 149 (1–2), 85–102.

Bachmann, O., Miller, C.F., de Silva, S.L., 2007. The volcanic–plutonic connection as a stage for understanding crustal magmatism. J. Volcanol. Geoth. Res. 167 (1–4), 1–23.

Bacon, C.R., Lowenstern, J.B., 2005. Late Pleistocene granodiorite source for recycled zircon and phenocrysts in rhyodacite lava at Crater Lake, Oregon. Earth Planet. Sci. Lett. 233 (3–4), 277–293.

Biswas, S., Coutand, I., Grujic, D., Hager, C., Stockli, D., Grasemann, B., 2007. Exhumation and uplift of the Shillong plateau and its influence on the eastern Himalayas: new constraints from apatite and zircon (U–Th–[Sm])/He and apatite fission track analyses. Tectonics 26 (6).

Briden, J.C., Rex, D.C., Faller, A.M., Tomblin, J.F., 1979. K–Ar geochronology and paleomagnetism of volcanic-rocks in the Lesser Antilles Island Arc. Philos. Trans. R. Soc. Lond. A Math. Phys. Eng. Sci. 291 (1383), 485–528.

Burke, K., 1988. Tectonic evolution of the Caribbean. Annu. Rev. Earth Planet. Sci. 16, 201–230.

Cherniak, D.J., Watson, E.B., 2003. Diffusion in zircon. Zircon 53, 113–143.

Claiborne, L.L., Miller, C.F., Flanagan, D.M., Wooden, J.L., Clynne, M.A., 2009. Geochronology of Zircon Surfaces Enhances the Record of Magma Storage and Recycling Beneath Mount St. Helens AGU Fall Meeting. American Geophysical Union, San Francisco.

Coleman, D.S., Gray, W., Glazner, A.F., 2004. Rethinking the emplacement and evolution of zoned plutons: geochronologic evidence for incremental assembly of the Tuolumne Intrusive Suite, California. Geology 32 (5), 433–436.

De Kerneizon, M.L., Bellon, H., Carron, J.P., Maury, R.C., 1983. The island of St-Lucia — petrochemistry and geochronology of the main magmatic series. Bull. Soc. Geol. France 25 (6), 845–853.

DeMets, C., Jansma, P.E., Mattioli, G.S., Dixon, T.H., Farina, F., Bilham, R., Calais, E., Mann, P., 2000. GPS geodetic constraints on Caribbean–North America plate motion. Geophys. Res. Lett. 27 (3), 437–440.

Deplus, C., Le Friant, A., Boudon, G., Komorowski, J.C., Villemant, B., Harford, C., Segoufin, J., Cheminee, J.L., 2001. Submarine evidence for large-scale debris avalanches in the Lesser Antilles Arc. Earth Planet. Sci. Lett. 192 (2), 145–157.

Devine, J.D., 1995. Petrogenesis of the basalt–andesite–dacite association of Grenada, Lesser Antilles island arc, revisited. J. Volcanol. Geoth. Res. 69 (1–2), 1–33.

Dodson, M.H., Compston, W., Williams, I.S., Wilson, J.F., 1988. A search for ancient detrital zircons in Zimbabwean sediments. J. Geol. Soc. 145, 977–983.

Eichelberger, J.C., Chertkoff, D.G., Dreher, S.T., Nye, C.J., 2000. Magmas in collision: rethinking chemical zonation in silicic magmas. Geology 28 (7), 603–606.

Farley, K.A., Kohn, B.P., Pillans, B., 2002. The effects of secular disequilibrium on (U–Th)/He systematics and dating of Quaternary volcanic zircon and apatite. Earth Planet. Sci. Lett. 201 (1), 117–125.

Fletcher, J.M., Grove, M., Kimbrough, D., Lovera, O., Gehrels, G.E., 2007. Ridge-trench interactions and the Neogene tectonic evolution of the Magdalena shelf and southern Gulf of California: insights from detrital zircon U–Pb ages from the Magdalena fan and adjacent areas. Geol. Soc. Am. Bull. 119 (11–12), 1313–1336.

Grunder, A.L., Klemetti, E.W., Feeley, T.C., McKee, C.M., 2006. Eleven million years of arc volcanism at the Aucanquilcha Volcanic Cluster, Northern Chilean Andes: implications for the life span and emplacement of plutons. Trans. R. Soc. Edinburgh-Earth Sci. 97, 415–436.

Harrison, T.M., Watson, E.B., Aikman, A.B., 2007. Temperature spectra of zircon crystallization in plutonic rocks. Geology 35 (7), 635–638.

Kay, S.M., Kay, R.W., 1985. Role of crystal cumulates and the oceanic-crust in the formation of the lower crust of the Aleutian Arc. Geology 13 (7), 461–464.

Lindsay, J.M., 2005. Saint Lucia. In: Lindsay, J.M., Robertson, R.E.A., Shepherd, J.B., Ali, S. (Eds.), Volcanic Hazard Atlas of the Lesser Antilles. Seismic Research Centre, The University of the West Indies, Trinidad and Tobago, pp. 218–238.

Macdonald, R., Hawkesworth, C.J., Heath, E., 2000. The Lesser Antilles volcanic chain: a study in arc magmatism. Earth-Sci. Rev. 49 (1–4), 1–76.

Matzel, J.E.P., Bowring, S.A., Miller, R.B., 2006. Time scales of pluton construction at differing crustal levels: examples from the Mount Stuart and Tenpeak intrusions, North Cascades, Washington. Geol. Soc. Am. Bull. 118 (11–12), 1412–1430.

Michel, J., Baumgartner, L., Putlitz, B., Schaltegger, U., Ovtcharova, M., 2008. Incremental growth of the Patagonian Torres del Paine laccolith over 90 k.y. Geology 36 (6), 459–462.

Miller, J.S., Matzel, J.E.P., Miller, C.F., Burgess, S.D., Miller, R.B., 2007. Zircon growth and recycling during the assembly of large, composite arc plutons. J. Volcanol. Geoth. Res. 167 (1–4), 282–299.

Paces, J.B., Miller Jr., J.D., 1993. Precise U–Pb ages of Duluth Complex and related mafic intrusions, northeastern Minnesota; geochronological insights to physical, petrogenetic, paleomagnetic, and tectonomagnetic processes associated with the 1.1 Ga Midcontinent Rift System. J. Geophys. Res., B, Solid Earth Planets 98 (8), 13,997–14,013.

Perfit, M.R., Brueckner, H., Lawrence, J.R., Kay, R.W., 1980. Trace-element and isotopic variations in a zoned pluton and associated volcanic-rocks, Unalaska Island, Alaska — a model for fractionation in the Aleutian Calcalkaline Suite. Contrib. Mineral. Petrol. 73 (1), 69–87.

Press, W.H., Flannery, B.P., Teukolsky, S.A., Vetterling, W.T., 1988. Numerical Recipes in C: the Art of Scientific Computing. Cambridge University Press, New York.

Reid, M.R., Coath, C.D., Harrison, T.M., McKeegan, K.D., 1997. Prolonged residence times for the youngest rhyolites associated with Long Valley Caldera; ^{230}Th–^{238}U ion microprobe dating of young zircons. Earth Planet. Sci. Lett. 150 (1–2), 27–39.

Roobol, M.J., Wright, J.V., Smith, A.L., 1983. Calderas or gravity-slide structures in the Lesser Antilles Island-Arc. J. Volcanol. Geoth. Res. 19 (1–2), 121–134.

Samper, A., Quidelleur, X., Boudon, G., Le Friant, A., Komorowski, J.C., 2008. Radiometric dating of three large volume flank collapses in the Lesser Antilles Arc. J. Volcanol. Geoth. Res. 176 (4), 485–492.

Schaltegger, U., Brack, P., Ovtcharova, M., Peytcheva, I., Schoene, B., Stracke, A., Marocchi, M., Bargossi, G.M., 2009. Zircon and titanite recording 1.5 million years of magma accretion, crystallization and initial cooling in a composite pluton (southern Adamello batholith, northern Italy). Earth Planet. Sci. Lett. 286 (1–2), 208–218.

Schmitt, A.K., Grove, M., Harrison, T.M., Lovera, O., Hulen, J., Walters, M., 2003a. The Geysers–Cobb Mountain Magma System, California (Part 2): timescales of pluton emplacement and implications for its thermal history. Geochim. Cosmochim. Acta 67 (18), 3443–3458.

Schmitt, A.K., Grove, M., Harrison, T.M., Lovera, O., Hulen, J., Walters, M., 2003b. The Geysers–Cobb Mountain Magma System, California (Part 1): U–Pb zircon ages of volcanic rocks, conditions of zircon crystallization and magma residence times. Geochim. Cosmochim. Acta 67 (18), 3423–3442.

Schmitt, A.K., Stockli, D.F., Hausback, B.P., 2006. Eruption and magma crystallization ages of Las Tres Vírgenes (Baja California) constrained by combined ^{230}Th/^{238}U and (U–Th)/He dating of zircon. J. Volcanol. Geoth. Res. 158 (3–4), 281–295.

Schmitt, A.K., Stockli, D.F., Niedermann, S., Hausback, B.P., 2010. Eruption ages of Las Tres Vírgenes volcano (Baja California): a tale of two helium isotopes. Quat. Geochron. doi:10.1016/j.quageo.2010.02.004

Siebert, L., Simkin, T., 2002. Volcanoes of the World: an Illustrated Catalog of Holocene Volcanoes and their Eruptions, Global Volcanism Program Digital Information Series. Smithsonian Institution.
Simon, J.I., Renne, P.R., Mundil, R., 2008. Implications of pre-eruptive magmatic histories of zircons for U–Pb geochronology of silicic extrusions. Earth Planet. Sci. Lett. 266 (1–2), 182–194.
Tomblin, J., 1964. The Volcanic History and Petrology of the Soufrière region, St. Lucia. University of Oxford, Oxford. 213 pp.
Turner, S., Hawkesworth, C., vanCalsteren, P., Heath, E., Macdonald, R., Black, S., 1996. U-series isotopes and destructive plate margin magma genesis in the Lesser Antilles. Earth Planet. Sci. Lett. 142 (1–2), 191–207.
Watson, E.B., Harrison, T.M., 1983. Zircon saturation revisited; temperature and composition effects in a variety of crustal magma types. Earth Planet. Sci. Lett. 64 (2), 295–304.
White, S.M., Crisp, J.A., Spera, F.J., 2006. Long-term volumetric eruption rates and magma budgets. Geochem. Geophys. Geosyst. 7.
Wiedenbeck, M., Alle, P., Corfu, F., Griffin, W.L., Meier, M., Oberli, F., Vonquadt, A., Roddick, J.C., Speigel, W., 1995. 3 natural zircon standards for U–Th–Pb, Lu–Hf, trace-element and Ree analyses. Geostand. Newslett. 19 (1), 1–23.
Wilson, C.J.N., Charlier, B.L.A., 2009. Rapid rates of magma generation at contemporaneous magma systems, Taupo Volcano, New Zealand: insights from U–Th model-age spectra in zircons. J. Petrology 50 (5), 875–907.
Wohletz, K., Heiken, G., Ander, M., Goff, F., Vuataz, F.D., Wadge, G., 1986. The Qualibou Caldera, St-Lucia, West-Indies. J. Volcanol. Geoth. Res. 27 (1–2), 77–115.
Wright, J.V., Roobol, M.J., Smith, A.L., Sparks, R.S.J., Brazier, S.A., Rose, W.I., Sigurdsson, H., 1984. Late Quaternary explosive silicic volcanism on St-Lucia, West-Indies. Geol. Mag. 121 (1), 1–15.